

Investigating Alaskan methane and carbon dioxide fluxes using measurements from the CARVE tower

A. Karion^{1,2,*}, C. Sweeney^{1,2}, J. B. Miller^{1,2}, A. E. Andrews², R. Commane³, S. Dinardo⁴, J. M. Henderson⁵, J. Lindaas^{3,**}, J. C. Lin⁶, K. A. Luus^{7,†}, T. Newberger^{1,2}, P. Tans², S. C. Wofsy³, S. Wolter^{1,2}, and C. E. Miller⁴

[1]{University of Colorado, Boulder, CO, USA}

[2]{NOAA Earth System Research Laboratory, Global Monitoring Division, Boulder, CO, USA}

[3]{School of Engineering and Applied Sciences, Harvard University, Cambridge, MA, USA}

[4]{Jet Propulsion Laboratory, Pasadena, CA, USA}

[5]{Atmospheric and Environmental Research, Lexington, MA, USA}

[6]{Atmospheric Sciences, University of Utah, Salt Lake City, UT, USA}

[7]{Biogeochemical Integration, Max Planck Institute for Biogeochemistry, Jena, Germany}

[*]{now at: National Institute of Standards and Technology, Gaithersburg, MD, USA}

[**]{now at: Colorado State University, Fort Collins, CO, USA}

[†]{now at: Dublin Institute of Technology, Dublin, Ireland}

Correspondence to: A. Karion (Anna.Karion@nist.gov)

Abstract

Northern high-latitude carbon sources and sinks, including those resulting from degrading permafrost, are thought to be sensitive to the rapidly warming climate. Because the near-surface atmosphere integrates surface fluxes over large (~500-1000 km) scales, atmospheric monitoring of carbon dioxide (CO₂) and methane (CH₄) mole fractions in the daytime mixed

1 layer is a promising method for detecting change in the carbon cycle throughout boreal
2 Alaska. Here we use CO₂ and CH₄ measurements from a NOAA tower 17 km north of
3 Fairbanks AK, established as part of NASA's Carbon in Arctic Reservoirs Vulnerability
4 Experiment (CARVE), to investigate regional fluxes of CO₂ and CH₄ for 2012-2014. CARVE
5 was designed to use aircraft and surface observations to better understand and quantify the
6 sensitivity of Alaskan carbon fluxes to climate variability. We use high-resolution
7 meteorological fields from the Polar Weather Research and Forecasting (WRF) model
8 coupled with the Stochastic Time-Inverted Lagrangian Transport model (hereafter, WRF-
9 STILT), along with the Polar Vegetation Photosynthesis and Respiration Model
10 (PolarVPRM), to investigate fluxes of CO₂ in boreal Alaska using the tower observations,
11 which are sensitive to large areas of central Alaska. We show that simulated
12 PolarVPRM/WRF-STILT CO₂ mole fractions show remarkably good agreement with tower
13 observations, suggesting that the WRF-STILT model represents the meteorology of the region
14 quite well, and that the PolarVPRM flux magnitudes and spatial distribution are generally
15 consistent with CO₂ mole fractions observed at the CARVE tower. One exception to this
16 good agreement is that during the fall of all three years, PolarVPRM cannot reproduce the
17 observed CO₂ respiration. Using the WRF-STILT model, we find that average CH₄ fluxes in
18 boreal Alaska are somewhat lower than flux estimates by Chang et al. (2014) over all of
19 Alaska for May-September 2012; we also find enhancements appear to persist during some
20 wintertime periods, augmenting those observed during the summer and fall. The possibility of
21 significant fall and winter CO₂ and CH₄ fluxes underscores the need for year-round in-situ
22 observations to quantify changes in boreal Alaskan annual carbon balance.

23

24 **1 Introduction**

25 The carbon cycle of the high northern latitudes has been the subject of study and research for
26 many decades (Harriss et al., 1992; Oechel et al., 1993; Walter et al., 2007; McGuire et al.,
27 2010; Olefeldt et al., 2013), with scientists and policy makers more recently focused on its
28 impact on global climate. This focus is in part due to the fact that global warming has
29 affected temperatures in the high northern latitudes more significantly than any other region
30 (IPCC, 2013). Higher temperatures could lead to a positive feedback of increased terrestrial
31 emissions of CO₂ and CH₄ (McGuire et al., 2009; O'Connor et al., 2010; Hayes et al., 2014;
32 Schuur et al., 2015), including a possibility of large emissions from thawing Arctic

1 permafrost. However, the timing and magnitude of such a feedback remain uncertain (Schuur
2 et al., 2008; Schuur et al., 2009; Schuur et al., 2015), and analysis of CH₄ and CO₂
3 measurements from the Global Greenhouse Gas Reference Network (GGGRN;
4 www.esrl.noaa.gov/gmd/ccgg) do not yet show signs of enhanced Arctic to mid-latitude
5 gradients (Bruhwiler et al., 2014; CarbonTracker, 2013). Planned future studies of ecosystems
6 and carbon cycling in Arctic and boreal regions are intended to monitor changes in climate
7 and carbon fluxes (e.g. NASA's Arctic-Boreal Vulnerability Experiment (ABoVE),
8 above.nasa.gov; Next-Generation Ecosystem Experiments (NGEE) Arctic, [ngee-
arctic.ornl.gov](http://ngee-
9 arctic.ornl.gov)). To this end, quantification of current carbon fluxes from the northern high
10 latitudes, including Alaska, is a crucial piece of any effort to detect changes in the Arctic and
11 boreal carbon cycle.

12 The Carbon in Arctic Reservoirs Vulnerability Experiment (CARVE) was a 5-year NASA
13 Earth Ventures (EV-1) airborne science investigation to quantify atmospheric mole fractions
14 and surface-atmosphere fluxes of CO₂ and CH₄ and correlate these with key surface-state
15 variables for terrestrial ecosystems in Arctic and boreal Alaska. In this region, both CO₂ and
16 CH₄ fluxes are dominated by the terrestrial biosphere; CH₄ fluxes in particular are dominated
17 by wetland emissions (Kirschke et al., 2013; Bruhwiler et al., 2014). Fossil fuel emissions are
18 concentrated in urban areas and in parts of the North Slope associated with oil exploration and
19 production near Prudhoe Bay. Studies have also shown some contribution to CH₄ emissions
20 from ebullition from lakes, a source not usually included in wetland inventories (Walter et al.,
21 2007). CARVE's goal is to bridge critical gaps in our knowledge and understanding of
22 Arctic-boreal ecosystems, linkages between the hydrologic and terrestrial carbon cycles, and
23 the feedbacks from disturbances such as thawing permafrost and fires. The principal
24 components of CARVE were the intensive aircraft campaigns conducted monthly from March
25 to November for four consecutive years (2012 – 2015). The aircraft payload included in-situ
26 sensors measuring CO₂, CH₄, and carbon monoxide (CO) throughout the flights, which are
27 based out of the Fairbanks airport and cover several regions throughout Alaska (Chang et al.,
28 2014). A stationary tower-based GHG measurement site, the CARVE tower (NOAA site
29 code CRV), was established as part of the CARVE project, in order to give year-round
30 context to the intensive aircraft observations. These continuous observations from a single
31 location can verify the temporal pattern of carbon cycle models, while the aircraft
32 observations provide information on spatial accuracy.

1 Measurements of CO₂ and CH₄ from towers in northern high latitudes have previously been
2 used to analyze emissions and trends in these regions (Sasakawa et al., 2010; Winderlich et
3 al., 2010; Worthy et al., 2015). Concentration measurements from such towers generally have
4 large regions of influence, on scales of hundreds of kilometers, in contrast to direct flux
5 measurements from eddy covariance flux tower sites, which may represent spatial scales
6 closer to tens or hundreds of meters, or chamber measurements that typically represent even
7 smaller (~1-meter) scales. In this sense, the tall tower measurements are able to integrate
8 fluxes that have been shown to be spatially heterogeneous (Olefeldt et al., 2013). Such
9 concentration or mole fraction measurements require interpretation using a model framework
10 to quantify terrestrial fluxes, because they do not measure them directly.

11 One way to infer and assess fluxes from mole fraction observations is to use a Lagrangian
12 particle dispersion model (LPDM) coupled with a meteorological model to determine the
13 influence function, or footprint, of a given observation (Lin et al., 2012). In this study, the
14 WRF-STILT modeling framework has been used to generate footprints for CARVE tower
15 observations. Henderson et al. (2015) provide details of the model configuration and
16 validation of the meteorological simulations. We assess CO₂ fluxes from the land surface of
17 Alaska by convolving surface fluxes from the PolarVPRM (Luus and Lin, 2015) with the
18 footprints and comparing the resulting modeled CO₂ enhancements with tower observations.
19 To infer CH₄ fluxes, we have convolved the footprints with a constant (in space and time)
20 flux model and an elevation-based flux model and scaled the results to monthly mean
21 observed enhancements to estimate monthly average fluxes over a wide region, using similar
22 methods as Chang et al. (2014).

23 In the following sections, we describe the CARVE tower site, its location, and region of
24 influence (Sect. 2). We then describe the measurement methods and the models used to infer
25 CO₂ and CH₄ fluxes (Sect. 3). We present the results in Sect. 4, and conclusions, including
26 future directions, in Sect. 5.

27 **2 Site overview**

28 **2.1 Site location**

29 The CARVE tower site was established in October 2011, 17 km north of Fairbanks, AK,
30 using an existing 32 m tower at the NOAA National Environmental Satellite, Data, and
31 Information Service (NESDIS) facility in Fox, AK (64.986°N, 147.598°W, ground elevation

1 611 m above sea level (asl); Fig. 1). The tower was chosen for its high elevation compared to
2 the immediate surrounding mean ground level and its relatively large region of influence, to
3 provide temporal and spatial context for CARVE aircraft measurements in interior Alaska.
4 The site was also chosen to satisfy logistical requirements, specifically that the site be easily
5 accessible year-round, and that the site be in a location that the CARVE aircraft could sample
6 over or close to during its campaigns without impacting the flight schedules or science
7 mission of each flight. NOAA/NESDIS personnel are stationed in a NESDIS office 5 km
8 from the road-accessible tower, providing technical support and high-speed Internet
9 connectivity throughout the year.

10 The surrounding land cover (within a 20-km radius, approximately the region shown in Fig.
11 1b) is composed of deciduous and evergreen forest, shrub/scrub, some scattered areas of
12 woody wetlands, mainly south of the Chena River south of Fairbanks, and medium and low-
13 intensity developed land in and immediately around Fairbanks (population 32,000) (2011
14 USGS National Land Cover Database (NLCD) (Homer et al., 2015)). The tower is located on
15 a ridge, and measurements from the tower represent a wide region of interior Alaska,
16 however, as indicated by surface influence fields generated from the WRF-STILT modeling
17 framework (Henderson et al., 2015), which show that the tower's influence region
18 encompasses a substantial part of Alaska (Fig. 1a).

19 **3 Methods**

20 **3.1 Measurements**

21 Three separate measurement systems for trace gases are deployed at the CRV tower site.
22 Programmable flask packages (PFPs) are used to collect air samples from the top level of the
23 tower at 32 m above ground level (agl), daily during the CARVE flight season (April –
24 October) and twice weekly during the remainder of the year (November – March).
25 Additionally, measurements of $^{14}\text{CH}_4$ are made from large-volume (~1000 L) whole-air
26 samples collected approximately biweekly, also from the 32 magl level. Lastly, continuous
27 in-situ measurements of CO_2 , CH_4 , and CO are made by drawing air from three heights (32
28 m, 17 m, and 5 m) through a Picarro G2401-m or G2401 Cavity Ring-Down Spectroscopic
29 (CRDS) analyzer. In addition to the measurements described above, a two-dimensional (2D)
30 sonic anemometer was deployed at the top of the tower and was operational from April 2012

1 through June 2014. Here we describe the continuous CO₂, CH₄ and CO measurements made
2 from October 2011 through the present, focusing on the calendar years 2012-2014.

3 Two different CRDS units have been deployed at the site as part of the CARVE project: SN
4 CFKBDS-2008 (model G2401-m, October 2011 – June 2013 and November 2014 – January
5 2015), and SN CFKADS-2067 (model G2401, June 2013 – October 2014 and January 2015 –
6 present). The only differences between the two units as configured at the site are the flow
7 rates (~550 standard cubic centimeters per minute (sccm) for CFKBDS-2008 and ~250 sccm
8 for CFKADS-2067) and their precision, defined here as the standard deviation of 30-second
9 averages, in measuring CO (1.3 ppb for CFKBDS-2008 and 4.3 ppb for CFKADS-2067).
10 Analyzer precision for CO₂ and CH₄ is the same for both analyzers (0.03 ppm and 0.2 ppb,
11 respectively).

12 The CRDS analyzer draws air through 0.635 cm (0.25 inch) outer diameter (OD) tubing
13 (Synflex 1300) with three different inlets installed at different heights above ground level:
14 31.7 m (level 3), 17.1 m (level 2), and 4.9 m (level 1). The analyzer primarily draws from the
15 highest level (level 3) for 50 minutes out of every hour, and then draws air for 5 minutes from
16 each of the other levels, operating on an hourly cycle. In our analysis, we use measurements
17 only from the top level, using measurements from level 2 to filter observations with large
18 vertical gradients (section 3.4); level 1 observations are not used. Measurements are discarded
19 for a time equivalent to three flushing volumes of the line (approximately 3 minutes) after a
20 level switch or a switch to or from a calibration tank, to allow each line to flush, because there
21 is no separate flushing of the lines during calibrations. The sample air is not dried, and a water
22 correction to the measurements is made in post-processing. The instrument-specific water
23 correction is based on a laboratory experiment conducted prior to deployment of each
24 analyzer, using methods described in Chen et al. (2013) and Rella et al. (2013). Data is
25 collected via serial communications on a Campbell Scientific CR1000 data logger along with
26 all auxiliary measurements (room temperature, line pressure, tank pressures, sonic
27 anemometer measurements of temperature and 2D winds), and averaged at 30-second
28 increments prior to remote collection via the Internet connection provided by
29 NOAA/NESDIS.

30 Two standard reference gases, calibrated against NOAA standards on the WMO scales for all
31 three gases, are each sampled every 8 hours for 5 minutes. Mole fraction measurements of
32 CO₂, CH₄, and CO are first corrected using a linear fit to either 5 or 6 NOAA reference tanks

1 from a calibration performed in the laboratory prior to each analyzer deployment, and then
2 drift-corrected using the measurements of the two tanks at the site. The average offset
3 (difference between corrected value and the actual tank value) is used for an offset drift
4 correction. The two on-site tanks are at two different mole fractions for each gas (373 and
5 409 ppm CO₂; 1818 and 2087 ppb CH₄; 177 and 284 ppb CO), so that if either the slope of
6 the correction changes, or one tank has significant drift, the measurements would show
7 increasing residuals with time. All measurements are reported here on the WMO scales for
8 each gas (CO₂ X2007, CH₄ X2004, and CO X2004, (Dlugokencky et al., 2005; Zhao and
9 Tans, 2006)). At CRV, the water correction uncertainty is estimated to be 0.1 ppm for CO₂,
10 0.5 ppb for CH₄, and 4 ppb for CO, based on analysis by Chen et al. (2013) for CO and Rella
11 et al. (2013) for CO₂ and CH₄, and is independent of other variables, including water vapor.
12 Comparisons of measurements from whole air samples in PFPs during low-variability periods
13 show differences (median ± 1-sigma) of -0.11±0.44 ppm, 0.8±1.2 ppb, and -1.3±4.5 ppb for
14 CO₂, CH₄, and CO, respectively, over the entire 3-year period. Total uncertainty
15 (reproducibility and comparability to other NOAA network sites) of hourly mole fraction
16 measurements at the site are generally <0.2 ppm, 2 ppb, and 5 ppb for CO₂, CH₄, and CO,
17 respectively (1-sigma), based on comparisons with flasks and residuals of the calibration
18 correction.

19 **3.2 Polar WRF – STILT Model**

20 The scientific analysis of CARVE atmospheric trace gas measurements is enabled through use
21 of the Stochastic Time-Inverted Lagrangian Transport (STILT) particle dispersion model (Lin
22 et al., 2003) coupled to the Polar variant version 3.5.1 (Wilson et al., 2011) of the Advanced
23 Research version of the Weather Research and Forecasting (WRF-ARW (Skamarock et al.,
24 2008)) numerical weather prediction model. The WRF-STILT modeling framework has been
25 used in many studies to estimate GHG emissions using airborne, surface, and tower-based
26 observations (Kort et al., 2008; Jeong et al., 2013; Chang et al., 2014; Miller et al., 2014;
27 McKain et al., 2015). Atmospheric dispersion in the LPDM is simulated by advecting tracer
28 particles by the three-dimensional gridded wind field from the WRF model, plus a turbulent
29 velocity component represented as a stochastic process (Markov chain) (Lin et al., 2003).
30 Time-averaged mass fluxes and convective mass fluxes from WRF are used in the dispersion
31 calculations (Nehrkorn et al., 2010). For each observation location (i.e. “receptor”), STILT
32 produces a two-dimensional surface influence field called a “footprint” (units of ppm / (μmol

1 $\text{m}^{-2} \text{s}^{-1}$)) that quantifies the influence of upwind surface fluxes on atmospheric concentrations
2 measured at the receptor location. The footprint field is proportional to the number of
3 particles in a surface-influenced volume (defined as the lower half of the planetary boundary
4 layer) and the time spent in that volume (Lin et al., 2003). As utilized in the current study, the
5 footprint can be multiplied by an *a priori* flux field (units of $\mu\text{mol m}^{-2} \text{s}^{-1}$) and integrated over
6 space and time to give the incremental contribution to the mole fraction (units of ppm) as
7 measured at the receptor location. The CARVE Polar WRF configuration consists of a triply
8 nested grid, with the innermost domain covering mainland Alaska on a 3.3-km grid to take
9 advantage of the improved representation at this scale of the underlying topography in this
10 region of significant orography. The STILT model runs over the entire WRF domain (all three
11 grids); footprints are gridded separately from WRF in post-processing over the whole domain
12 (30°N - 90°N and 180°E - 180°W). The reader is directed to Henderson et al. (2015) for more
13 detail and validation of the meteorological fields.

14 STILT footprints used for this analysis were generated every 3 hours during local nighttime
15 and hourly during local daytime, for a total of 16 footprints per day, and gridded at $0.5^\circ \times 0.5^\circ$
16 resolution. For each footprint, 500 particles were emitted from the tower location and altitude
17 above sea level and traced backwards in time for 10 days. The altitude above sea level rather
18 than ground level was used for the location of the particle emission because the elevation of
19 the model grid cell containing the tower site was significantly lower than the actual elevation
20 of the site (343 masl vs. 611 masl), despite use of the high-resolution grid (Henderson et al.,
21 2015). To reduce biases induced by differences in actual and modeled topography, we use
22 footprints generated during mid-afternoon hours (1 pm to 6 pm local Alaska standard time
23 (LST), UTC+8) only for our analysis, except where noted specifically. During these hours,
24 the lower atmosphere is generally well-mixed, and the difference between the mole fractions
25 measured at the top level (32 magl) and the middle level (17 magl) average between -0.25 and
26 0.25 ppm for CO_2 and -0.2 and 0.3 ppb for CH_4 (maximum monthly averages for the whole
27 time series), indicating good mixing and only a small influence from nearby sources that
28 would cause a near-surface gradient.

29 We also compared measurements from the top level of the tower to CARVE aircraft
30 measurements made above the tower site, generally during the months of March to October.
31 We compared aircraft measurements of CO_2 and CH_4 that were made below 2000 masl (1389
32 magl) and within 0.2 degrees in latitude and longitude of the tower, between the hours of 1

1 pm and 6 pm LST. This allowed us to determine how well measurements made from the top
2 level of the tower represent planetary boundary layer (PBL) average mole fractions during
3 those times. Differences between the 29 aircraft observations and tower-based hourly means
4 were -0.6 ± 2.0 ppb CH₄ and 0.3 ± 0.9 ppm CO₂ (mean \pm 1-sigma) during the March-October
5 air campaign period, indicating that the hourly average mole fractions at the tower are
6 generally representative of average mole fractions in the PBL.

7 We expect, based on the measured gradients at the tower and the comparison with aircraft
8 measurements above the tower, that during local mid-afternoon periods the tower
9 measurements closely represent measurements within a well-mixed PBL, and that during
10 those times, the impact of the height difference between the modeled site elevation and the
11 real site elevation is minimized. In our flux analysis, described in the following sections, we
12 also specifically filter out hourly averages during which the absolute value of the mole
13 fraction gradient between 17 and 32 magl levels in CH₄ is larger than 2 ppb.

14 We performed a sensitivity analysis on the transport model by examining footprints generated
15 at 300 magl (the default, or 611 masl) with those generated at 100 magl and 35 magl. We
16 found that the footprint influence from March to September of all three years was increased
17 by a small amount, resulting in estimated CH₄ fluxes (Section 3.5) that were 5-9% lower.
18 The effect was greater in winter months, however, affecting our flux estimates by 12-17%
19 using the 100 magl runs and by 26-32% using the 35 magl runs (again, decreasing the fluxes
20 due to increased surface influence). These differences were calculated only based on
21 observations used in the flux analysis, i.e. filtered for large vertical gradients as described
22 above. Although CH₄ fluxes reported in Section 4.5 were estimated using the footprints from
23 the higher 300 magl altitude, reflecting the true 611 masl altitude of the observations, this
24 sensitivity analysis indicates that uncertainty in modeled transport is greater in winter months.
25 We have added (in quadrature) the mean summer and winter differences for each year
26 between the analysis at 35 and 300 magl to the flux estimates for CH₄ in Section 3.5.

27 **3.3 Calculation of background mole fractions**

28 To compare the mole fraction variability and enhancements at CRV tower to those from the
29 modeling framework, it is necessary to determine the appropriate background mole fractions
30 for both CO₂ and CH₄. We derive background mole fractions using the particle trajectories
31 from the STILT runs and a data-based Pacific basin boundary “curtain” derived from

1 NOAA/ESRL Global Monitoring Division GGGRN measurements using an approach similar
2 to the one described in Jeong et al. (2013) and Miller et al. (2014). Specifically, the boundary
3 curtain is constructed using GGGRN surface and aircraft vertical profile CO₂ and CH₄
4 observations (Sweeney et al. (2015) and www.esrl.noaa.gov/gmd/ccgg/aircraft/) to create a
5 smoothed curtain representing the Pacific boundary. The curtain is a function of time,
6 latitude, and altitude. For each STILT run, the 500 particles are traced back in time until they
7 either exit a box defined by [170°W, 130°W] and [0°N, 75°N] or remain in the box for the
8 full 10-day run. All particles are then tagged with an exit time, longitude, latitude, and
9 altitude. Any particles whose final longitude is east of 160°W with a final latitude between
10 55 and 72°N and altitude below 3000 masl are removed in order to eliminate particles that did
11 not enter Alaska from either the western boundary or from high altitudes within the 10-days
12 of the observation. This filter is necessary because air masses that contain surface influence
13 from Canada or remain in Alaska for more than 10 days would not properly be represented by
14 the Pacific boundary as background. We note that the footprint itself is not changed by this
15 choice, but the particles that do not enter from the West are not used in the background
16 calculation. However, if a given 500-particle run has more than 25% of its particles
17 eliminated due to the above constraints, no background is computed for that hour, and
18 therefore no enhancement is computed either. This choice removes 50% of the hours from the
19 analysis over all three years. If at least 75% of the particles remain, these remaining particles
20 are tagged with the mole fraction from the Pacific boundary curtain at their exit latitude,
21 altitude, and time. The mole fractions for the particles are averaged to derive the background
22 mole fraction for the corresponding tower measurement and WRF-STILT footprint.

23 To understand the sensitivity of the CH₄ analysis to this choice of filtering for influence from
24 the east, we repeated the analysis with two additional background choices: one in which all
25 particles were tagged with a mole fraction, regardless of their origin, but the background was
26 only calculated if 75% or more particles originated in the west; and one for which all particles
27 were tagged and there was no filtering based on the percentage of particles not originating in
28 the west. We found that the difference in the background values was within the one-sigma
29 uncertainty in the background itself, calculated as described below. However, we found that
30 including hourly observations for which the air mass did not enter strictly from the West
31 generally reduced the monthly methane flux estimates by 9-30%; this result is discussed
32 further in Section 3.5.

1 Uncertainty in the background is determined similarly to Jeong et al. (2013): it is assigned the
2 quadrature sum of the standard error of the mean mole fraction (i.e. the standard deviation of
3 the particle mole fractions divided by the square root of the number of particles used) with the
4 average value of the root mean square (RMS) residuals of the empirical background curtain of
5 the particles. The RMS residuals of the curtain are calculated at every point along the curtain
6 (a function of latitude, altitude and time); they are the residuals of the curve fit that generates
7 the smoothed background curtain and the data that is used to generate the curve. Thus, it is a
8 quantification of uncertainty of the curtain itself. The background uncertainty in this work is
9 dominated by the RMS residuals of the boundary curtain component.

10 **3.4 CO₂ Flux Model**

11 The CO₂ measurements at the CRV tower were interpreted with the assistance of biospheric
12 CO₂ flux estimates generated by the Polar Vegetation Photosynthesis and Respiration Model
13 (PolarVPRM, (Luus and Lin, 2015)). PolarVPRM captures the strong diurnal and seasonal
14 variability of CO₂ fluxes parsimoniously, according to empirical associations between
15 environmental conditions and eddy covariance measurements of CO₂, and regionally across
16 Alaska (3-hourly, 1/6 x 1/4 degrees latitude x longitude), using data products from the North
17 American Regional Reanalysis (NARR) (Mesinger et al., 2006) and the Moderate Resolution
18 Imaging Spectroradiometer (MODIS). Subnivean and growing season respiration are
19 calculated as functions of NARR soil and air temperature, respectively; snow and growing
20 seasons are differentiated using MODIS snow cover (Riggs and Hall, 2011). Photosynthesis is
21 calculated as a function of NARR air temperature, NARR shortwave radiation, water
22 availability (via MODIS), and vegetation (via the MODIS enhanced vegetation index (Solano
23 et al., 2010)). The CO₂ fluxes from PolarVPRM were convolved with footprints from
24 observations at the tower to derive model-based enhancement above background (ΔCO_2) for
25 the 3-year period from 2012-2014. These modeled CO₂ enhancements were compared to CO₂
26 enhancements observed at CRV.

27 Hourly observations used for CO₂ analysis were restricted to periods between 1 pm and 6 pm
28 LST, to minimize discrepancies between real and modeled boundary layer dynamics. In
29 addition, as described above, samples that had no background determination for more than
30 25% of the released particles were omitted. Additional filters on the data were designed to
31 restrict analysis to periods when the PBL was most likely well mixed, as determined from the
32 vertical gradient in CH₄ mole fractions between the 17 m and 32 m levels; only data for which

1 the CH₄ vertical gradient was less than 2 ppb were retained. Also, only data observations
2 with low temporal variability were retained, determined as having a standard deviation of 30-
3 second measurements in an hour below 7 ppb in CO and 3 ppb in CH₄; this filter was applied
4 to reduce influence from local sources, a concern at this site because of the proximity of
5 Fairbanks. Lastly, biomass-burning (and some large pollution) events were filtered out by
6 removing observations for which the enhancement in CO (relative to the background
7 determined using methods described in Sect. 3.3) exceeded 20 ppb. The combined effect of
8 these filters and the background filter eliminated 56% of the days analyzed – most were
9 removed by the background filter described in Sect. 3.3. The filters described above were
10 used to filter data only for the CO₂ flux-model comparison analysis described in this section
11 with the results in Section 4.4, and for the CH₄ footprint and flux analyses described in
12 Sections 3.5 with results in Sections 4.5 and 4.6.

13 **3.5 CH₄ Flux Estimation**

14 In the CH₄ analysis, as for CO₂, only hourly average mole fractions between 1 pm and 6 pm
15 LST were used, with the same filters applied on the observations to limit instances of high
16 variability, large vertical gradients, and biomass burning, as outlined in Sect. 3.4. We also
17 carried out the analysis without the observational filters and did not find any difference in the
18 resulting monthly fluxes within the 1-sigma uncertainty of the background presented here,
19 with the exception of months with significant biomass burning events.

20 Chang et al. (2014) investigated the use of existing CH₄ flux models to interpret observations
21 from CARVE airborne campaigns and found that none of them performed better than the
22 assumption of a uniform flux. Hence, here we use two simple flux spatial distributions to
23 interpret the tower observations and estimate average CH₄ fluxes. The first flux map is a
24 uniform land-based flux (with oceanic flux set to zero, assuming the oceanic CH₄ flux
25 contribution is negligible (Kirschke et al., 2013)) similar to what was used in Chang et al.
26 (2014) to estimate CH₄ fluxes using aircraft observations from the 2012 CARVE campaign.
27 This model assumes a spatially constant flux over all land regions. The second flux map
28 pattern is based on elevation data from NOAA's NGDC,
29 (<http://www.ngdc.noaa.gov/mgg/topo/report/globedocumentationmanual.pdf>) (Fig. 1a). The
30 elevation map was averaged to the same spatial resolution as the footprints (0.5° x 0.5°) and
31 adjusted so that the ocean and elevations higher than 1000 masl were assumed to have zero

1 CH₄ flux. Elevations between 0 and 1000 masl were scaled linearly from 1 to 0, with areas of
2 zero elevation (including lakes) assigned 1 and 1000 masl assigned 0. Fluxes were assumed to
3 be diurnally constant. A third map based on elevation gradients (in which highly sloped
4 regions had less flux and flatter areas had higher flux) was also tested, but the results were
5 very similar to the elevation-based map, so they are not shown here.

6 Observed CH₄ enhancements relative to the footprint background were averaged over the
7 mid-afternoon hours (1 pm – 6 pm LST) to obtain daily averages. These daily enhancements
8 were then averaged to obtain monthly average ΔCH₄ values throughout each year. However,
9 in many winter months, fewer than 6 days of observations remained after the data filtering;
10 those months were omitted from the analysis. The constant flux map and the elevation-based
11 flux map were convolved with the hourly footprints from the WRF-STILT model to obtain
12 initial values of modeled ΔCH₄. These were then averaged to create daily values (with the
13 same filters as for the observations) and then to monthly values. The monthly flux maps were
14 then scaled to the observations, so that the simulated monthly ΔCH₄ matched the
15 observations. This method is equivalent to taking the mean of the individual daily flux
16 estimates (F_D) weighted by their corresponding footprints (I_D). For the case of unit flux, the
17 daily flux estimate (F_D) is the CH₄ enhancement (ΔCH₄) divided by the footprint influence:

$$18 \quad F_D = \frac{(\Delta CH_4)_D}{I_D}$$

19 The monthly average flux (F_M), is the average of the daily fluxes weighted by each day's
20 influence, which is equivalent to dividing an average methane enhancement by the average
21 monthly influence, I_M :

$$22 \quad F_M = \frac{\sum_D F_D I_D}{\sum_D I_D} = \frac{\overline{\Delta CH_{4,M}}}{I_M}$$

23 Uncertainties on monthly fluxes were determined from the background mole fraction
24 uncertainty and uncertainty based on a sensitivity analysis of influence functions calculated
25 using different heights in the model (Section 3.2). A formal transport uncertainty analysis
26 (e.g., error in PBL depth or wind speed) was not considered, but would likely increase the
27 errors shown here. Monthly background errors (Section 3.3) for CH₄ ranged from 2-7 ppb
28 (average 5 ppb), which was generally of the same order of magnitude as the CH₄

1 enhancements. Uncertainty on the monthly enhancements was calculated as the average of
2 the uncertainty on the background for each day divided by the square root of the number of
3 independent samples during that month, approximating the standard error of the monthly
4 mean enhancement. The correlation time scale of the background for CH₄ (after a 60-day
5 smoother was subtracted to eliminate the long-term temporal correlations) was approximated
6 at 9 days, consistent with synoptic-scale variability. The number of independent realizations
7 for each month was therefore derived as the number of days in that month divided by 9. This
8 represents a 1-sigma uncertainty estimate; the fractional uncertainty on the monthly CH₄
9 enhancement was then summed in quadrature with the uncertainty based on the altitude
10 sensitivity analysis and propagated to the monthly flux estimates.

11 A sensitivity analysis to the background filter, as described in Section 3.3, showed that the
12 background mole fractions were within the 1-sigma uncertainty when calculated using the two
13 additional background options. We did find, however, that the fluxes were generally 9-30%
14 lower when the observations with the bulk of the air mass not entering from the West were
15 included. We found that in this case, the average footprint influence was greater, likely
16 because the air masses spent more time over land. With no corresponding increase in
17 observed CH₄ enhancements, this led to a lower flux estimate on those days. However, the
18 CH₄ enhancements in this case have high uncertainties because it is very hard to estimate
19 what the background for those days might be.

20 **4 Results**

21 **4.1 Diurnal cycles**

22 The diurnal cycles of CO₂ and CH₄ at the tower have been analyzed over the study period,
23 2012-2014. All analysis shown is based on hourly-averaged measurements from the top-most
24 level at 32 magl. Measurements during times when the CO mole fraction exceeded 200 ppb
25 were removed to filter out the effect of large biomass burning events. No other filters were
26 applied on the data in this portion of the analysis. The diurnal cycle of CO₂ shows an
27 amplitude (maximum – minimum CO₂) of 10 ppm in July, with a wintertime (November-
28 April) magnitude of approximately 2 ppm (Fig. 2, top panel), with similar patterns each year.
29 CH₄ diurnal cycle amplitudes also show a maximum in summer (in either July or August,
30 depending on the year) between 20 and 30 ppb. The wintertime diurnal cycle of CH₄, driven
31 by boundary layer dynamics, shows an average amplitude of 10 ppb (Fig. 2, lower panel).

1 Shaded areas in Fig. 2 indicate the standard deviation of that month's average over all days in
2 the 3-year period, indicating significant variability in the amplitudes for both gases, and
3 especially for CH₄, where the amplitude variability (one-sigma) ranges from zero to 45 ppb.

4 The average amplitudes of the CH₄ and CO₂ diurnal cycles at the CARVE tower are
5 significantly smaller than those that have been reported at other Arctic and boreal
6 measurement sites. Worthy et al. (2015) compare diurnal cycle amplitudes of CH₄ at various
7 Arctic tower sites throughout Canada and North America, finding that summertime diurnal
8 CH₄ amplitudes at all the Arctic and boreal Canadian sites are significantly larger than at
9 CRV tower. Sasakawa et al. (2010; 2013) report larger CH₄ and CO₂ diurnal cycle
10 magnitudes as well from a network of Siberian tower sites. Winderlich et al. (2010) also
11 report similarly large diurnal cycle amplitudes in CH₄ (~200 ppb) and CO₂ (~25 ppm) from
12 the lower levels of the ZOTTO tall tower in boreal Siberia; however, at the highest level (301
13 magl) the average July 2009 diurnal cycle amplitude is significantly smaller at ~50 ppb CH₄
14 and ~5 ppm CO₂, presumably because the top of the night-time PBL is often below this tallest
15 level. This may be the case at CRV, which despite its low height above ground level, is
16 elevated above the surrounding area and does not observe high CH₄ mole fractions from
17 lower-elevation wetlands at night, as their emissions would be trapped in the shallow valleys
18 below the site. The CRV tower is surrounded by deciduous and evergreen forest, however, so
19 the CO₂ cycle is comparably larger. The diurnal cycle at the 17 magl and 5 magl levels is
20 slightly greater than at 32 magl in summer, but not significantly so (1-2 ppb larger for CH₄
21 and 1-2 ppm for CO₂ on average in July and August).

22 **4.2 Seasonality of winds and influence functions**

23 The mid-afternoon daily average footprints (the entire set of footprints, without applying a
24 background or other filter) from the WRF-STILT model were examined to determine the
25 influence of different regions on the measurements at the tower throughout the year. The total
26 magnitude of land-surface influence (ocean influence is not included) on the tower
27 measurements for each month of each of the three study years (2012, 2013, 2014) was
28 determined (Fig. 3), along with the total influence of several sub-regions: Canada (light blue,
29 Fig. 3), the North Slope of Alaska (defined as north of the Brooks Range, red, Fig. 3), the
30 remainder of Alaska (dark blue, Fig. 3), and Eurasia (yellow, Fig. 3). The seasonality of the
31 land surface influence is clear and consistent between all three years. Specifically, in all three
32 years, the months of May through September show significantly less land surface influence on

1 the tower than October through April. This stems from the smaller influence of Canada, and
2 to a lesser extent, lower Alaska, on the measurements during the summer months. The
3 influence of the Eurasian continent is very small throughout the years, but so is the influence
4 of the North Slope of Alaska. This is also apparent when the mid-afternoon footprint
5 influences are aggregated over seasons and years, as shown in the 80% influence range (Fig.
6 1a), which does not include the North Slope region. The footprint influence from the subset of
7 days used in the analysis in sections 4.4 and 4.5 is also shown in Fig. 1a, showing
8 correspondingly less influence from Canada, since the main filter applied removed days for
9 which significant portions of the air mass did not enter the domain from the West. Without a
10 good method for estimating background concentrations when winds are coming from the
11 eastern sector we are substantially limiting the potential of this tower to monitor fluxes from
12 the domain east of the site. From this analysis we also conclude that measurements at the
13 CRV tower are not substantially affected by emissions north of the Brooks Range, and any
14 emissions estimates made using the tower measurements will not apply to the North Slope.

15 Daytime wind measurements from the 2D sonic anemometer (from all days when it was
16 operational) at the tower support the finding of large seasonality in the footprints (Fig. 4).
17 Winds at the tower during May-September are predominantly from the west and southwest,
18 with some frequency of winds from the east as well. However, from October to April, the
19 winds are almost exclusively from the east/northeast. These wind directions support the
20 conclusion from the model influence functions that wintertime measurements are more
21 influenced by Canadian land than in summertime, as shown in Fig. 3. In addition, winds in
22 any season do not generally come from the North, supporting the lack of influence from the
23 North Slope. Similar seasonality and lack of northern influence was found in a recent
24 analysis of data from NOAA/ESRL Aircraft Network at Poker Flat, AK (Sweeney et al.,
25 2015).

26 **4.3 Background and Relative Enhancements of CH₄, CO₂, and CO**

27 The definition of an appropriate background is a crucial aspect of analyzing the CRV tower
28 CO₂ and CH₄ measurements. We calculate the background as described in Sect. 3.3, using
29 the particle back trajectories and the empirical Pacific boundary curtain, and refer to this as
30 the footprint background. We also compare this background to the value of the same Pacific
31 curtain at 3500 masl and 65°N, i.e. the free troposphere at the latitude of the tower. For CO₂
32 (middle panel, Fig. 5) the definition of the background does not have as large an effect as it

1 does for CH₄. For CH₄ (top panel, Fig. 5) the choice of background is crucial to any analysis
2 of the measurements, for two reasons. First, the CH₄ signal at CRV is relatively small
3 compared to the variability of the background. Second, the CH₄ background varies depending
4 on the latitudinal origin of the air mass, because of the large global latitudinal gradient in CH₄
5 (Dlugokencky et al., 2009). Comparison of the measurements with the footprint background
6 and free-tropospheric background (Fig. 5) illustrates that the footprint background varies at
7 synoptic time scales as air-mass origins change, and tracks the variability in the measurements
8 at the site. CH₄ enhancements over background are small and thus very sensitive to
9 background choice (top panel in Fig. 5). We note that despite the small signal, however, the
10 time series of CH₄ observations clearly shows both wintertime and summertime
11 enhancements, with wintertime enhancements sometimes correlated with CO enhancements
12 as well, indicating a possible anthropogenic source for these signals (see Sect. 4.6 and Table
13 1). Evidence of biomass burning events is also clear in all three species, but most easily
14 observed in the CO signals during the summers of 2012 and 2013.

15 **4.4 CO₂ Model-Observation Comparison**

16 Observations of monthly mean CO₂ relative to the background (ΔCO_2) show consistent
17 features from year to year (Fig. 6), with the sign of the enhancements showing the sign of the
18 monthly net CO₂ fluxes, or Net Ecosystem Exchange (NEE). Positive enhancements from
19 January-April indicate that respiration is occurring even during this coldest period of the year.
20 In addition, all years show the highest respiration signal in October, possibly indicative of
21 photosynthesis stopping while soil temperatures are still high enough to sustain significant
22 respiration, although some of this signal could also be due to the seasonality in vertical
23 mixing and/or winds. Although the maximum drawdown occurs in July and is of similar
24 magnitude in all years (~8 ppm), the transition from net respiration to net photosynthetic
25 uptake occurs earlier in 2014 (April) than in 2012 and 2013 (May). The timing and
26 magnitude of the ΔCO_2 observations relative to background represent a stringent test for the
27 transport and surface flux models.

28 The modeled ΔCO_2 from the convolution of WRF-STILT footprints with PolarVPRM fluxes
29 are compared to hourly averaged observed ΔCO_2 mole fractions at the tower during the mid-
30 afternoon in Figs. 6 and 7. (Note that the time series data in Fig. 6 (top) has not been filtered,
31 but the monthly averages in the lower panel and the data shown in Fig. 7 only use filtered

1 data.) Both the hourly time series and monthly average comparisons between modeled and
2 observed ΔCO_2 at the tower during mid-day hours indicate that the PolarVPRM fluxes and
3 WRF-STILT meteorology are able to reproduce the magnitude and timing of the tower CO_2
4 signal remarkably well during most seasons (Fig. 6). Hourly observations of ΔCO_2 that
5 satisfy the filtering conditions are well correlated with modeled ΔCO_2 in all three years (Fig.
6 7). The data close to the 1:1 line indicate that the magnitude of the fluxes is generally well
7 captured by the model. The correlations are strong in all three years ($R^2 = 0.61$ to 0.75),
8 indicating that the PolarVPRM CO_2 fluxes and the WRF-STILT transport model are able to
9 reproduce observed signals at the tower remarkably well with no adjustment to match the
10 data.

11 There are two exceptions apparent in otherwise the very good comparison between the model
12 and observations. First, monthly average ΔCO_2 observations compared to the model (Fig. 6,
13 lower panel) indicate that the PolarVPRM/WRF-STILT modeled NEE is slightly more
14 negative than observations in May and June in both 2012 and 2013, with an earlier spring
15 drawdown in the model than the observations suggest. However, in all of these months the
16 model results, with no uncertainty estimates, overlap with the one-sigma data uncertainty.
17 This difference is also observable in the correlations between modeled and observed ΔCO_2
18 (Fig. 7), with some data points with more negative ΔCO_2 in the model than in the
19 observations. Whether this small offset between model and observations results from
20 insufficient modeled respiration or too much modeled photosynthesis during the spring is
21 impossible to tell from CO_2 observations only. A second exception to the very good
22 agreement is that the model systematically underestimates the magnitude of the observed late
23 fall respiration flux (October to November) in all three years. This may be because model
24 respiration is calculated as a function of air temperature when per-pixel snow cover area is
25 $<50\%$, whereas actual rates of late fall respiration are influenced by microbial activity
26 sustained in the soil, which cools more gradually than the air. Despite these differences, the
27 overall good agreement between model and observations indicates that in addition to
28 capturing the magnitude, the PolarVPRM and WRF-STILT models are likely capturing most
29 of the timing and spatial structure of the fluxes in boreal Alaska as well.

30 **4.5 CH₄ Model-Observation Comparison**

31 The scaled monthly CH_4 fluxes from the elevation-based and uniform (constant) flux maps
32 were convolved with the WRF-STILT footprints corresponding to the observations. The

1 hourly ΔCH_4 from each model was compared with the observed enhancements (Fig. 8) for
2 each year. The elevation-based model enhancements (lower row, Fig. 8) match the data
3 slightly better than the uniform flux model (upper row, Fig. 8) in 2012 and 2014, but not
4 2013. We also investigated a third spatial flux map pattern that was based on the gradient in
5 elevation, but did not find any improvement in the correlations over the simpler elevation-
6 based and uniform flux models. Neither model was able to achieve good correlations
7 between the model and the observations, a conclusion that was also reached by Chang et al.
8 (2014) when they investigated multiple different CH_4 flux models. This result is in sharp
9 contrast to the high correlations achieved using the PolarVPRM CO_2 fluxes with the same
10 WRF-STILT footprints, leading to the conclusion that the WRF-STILT meteorology is able to
11 replicate observations when an accurate spatial flux map is used. Although the approximate
12 magnitude of the CH_4 enhancements is correct because of the monthly scaling, the large
13 spread and lack of correlation around the 1:1 line indicates that the model cannot replicate
14 hourly variability in enhancements, because the uniform spatial and temporal (we assume
15 constant monthly fluxes) representation is likely to be incorrect, and likely because of higher
16 relative uncertainty in the background.

17 **4.6 Average Scaled CH_4 Fluxes**

18 Monthly CH_4 fluxes from the uniform flux map were averaged over the state of Alaska to
19 obtain average fluxes for each month and for each year, and compared with the results from
20 (Chang et al., 2014) (Fig. 9). Results from the elevation-based flux map were statistically the
21 same as those from the uniform flux map and are not shown. CH_4 fluxes are small relative to
22 those determined from some flux tower or chamber-based studies in arctic wetlands
23 (Euskirchen et al., 2014; Johnston et al., 2014; Whalen and Reeburgh, 1988; Fan et al., 1992;
24 Olefeldt et al., 2013), but very similar in magnitude to CH_4 fluxes recently reported from a
25 black spruce forest during the snow-free seasons from 2011-2013 at a flux tower site in
26 Fairbanks, AK (Iwata et al., 2015), as well as those reported from the Zotino Tall Tower
27 Observatory (ZOTTO) in Siberia during the summers of 2009-2011 ($7.7 \text{ mg CH}_4 \text{ m}^{-2}\text{d}^{-1}$)
28 (Winderlich et al., 2014). They are also smaller than fluxes estimated by Chang et al. (2014)
29 using CARVE aircraft observations in the summer of 2012 (Fig. 9), but the two results
30 overlap within their 1-sigma uncertainty bands. One possible reason for the lower average
31 fluxes observed at the CARVE tower could be the region to which the CARVE tower
32 observations are sensitive in the summer. The CARVE tower observations do not capture

1 emissions over the North Slope of Alaska, where other studies have shown large (but highly
2 variable) CH₄ emissions, at least over small areas (Euskirchen et al., 2014; Morrissey and
3 Livingston, 1992; von Fischer et al., 2010; Olefeldt et al., 2013). The signal in CH₄ at CRV
4 may also be small because of the CARVE tower's large region of influence, which integrates
5 signals from a wide variety of ecosystems that have different flux profiles, including not only
6 low-lying wetlands and forests, but also extensive upland and mountain regions.

7 The tower observations also suggest the presence of non-zero fall and wintertime fluxes.
8 Mastepanov et al. (2008) observed a burst of CH₄ emissions in high-latitude wetlands in fall,
9 and, more recently, Zona et al. (2016) reported significant natural CH₄ fluxes persisting
10 through the late fall in the North Slope of Alaska; our results support the existence of late-fall
11 (September-October) CH₄ fluxes in the boreal zone as well. Additionally, our analysis also
12 suggests the presence of CH₄ emissions in late winter (January-March) in some years, ,
13 although this conclusion is uncertain and requires further investigation with a larger data set,
14 given the smaller data sample in our analysis in winter and the larger uncertainty associated
15 with modeled transport, as indicated by the sensitivity of the influence footprints to altitude
16 during winter months. To understand the role that fossil sources from nearby Fairbanks or
17 farther away might play, especially in winter, we analyze correlations between ΔCH_4 and
18 ΔCO mid-afternoon hourly enhancements. These enhancements indicate that some wintertime
19 CH₄ emissions are likely anthropogenic, with coefficients of determination (R^2) generally
20 larger in the winter months and close to zero in June, July and August of all years. Not all
21 winter months show high correlations, and May 2012 also has highly correlated ΔCH_4 and
22 ΔCO (Table 1).

23 We note that total uncertainty on the quantitative flux analysis presented here has not been
24 calculated, and would come from a number of components, including transport error in the
25 model. We also note that transport uncertainty is higher in the winter months, when the
26 elevation resolution in the model introduces a larger error than during spring and summer
27 periods. Here we have calculated the uncertainty of the observed enhancements, based on the
28 background uncertainty, and an estimate of the uncertainty associated with the model's
29 representation of the tower's ridge-top location based on our sensitivity analysis; this total is
30 still likely an underestimate of the total uncertainty of the flux estimates.

1 **5 Conclusions**

2 The CARVE tower, located on a ridge outside Fairbanks, is well situated to provide regional
3 year-round CO₂ and CH₄ observations that provide context to the CARVE aircraft campaign
4 measurements, which were made throughout Alaska from March to November from 2012 to
5 2015. The WRF-STILT transport model was used to determine the influence region of the
6 site and its inter-annual and seasonal variability. The model results showed significantly more
7 influence from the region east of the tower in wintertime, a pattern that was repeated in all
8 three years and was confirmed by anemometer data from the site. The model also indicated
9 that processes in the North Slope of Alaska have very little influence on the tower
10 observations. This seasonality of transport to the region has been previously documented
11 (Sweeney et al., 2015), and implies that additional long-term observing sites are required to
12 constrain Alaskan fluxes; a site in Western Alaska, for example, would be more likely to have
13 fluxes from interior Alaska in its observation footprint in the wintertime, and a site north of
14 the Brooks Range would be required to investigate fluxes from the North Slope.

15 We calculated enhancements of CO₂ and CH₄ during local mid-afternoon times by subtracting
16 a background also determined using the WRF-STILT model particle trajectories, and found
17 that the background choice is critical for CH₄, for which enhancements are very small, and of
18 the same order of magnitude as the uncertainties. CO₂ enhancements at the CARVE tower
19 site are replicated remarkably well by the WRF-STILT model when convolved with
20 PolarVPRM biogenic CO₂ fluxes (Luus and Lin, 2015), with a few noted exceptions. The
21 high correlation between modeled and observed CO₂ give confidence in the STILT footprints
22 and the WRF meteorological model that was used to generate them. The signal in CO₂ is
23 larger than that for CH₄, such that the background uncertainty is not as large relative to the
24 enhancements or depletions.

25 The WRF-STILT meteorological model enables us to constrain the magnitude of mean
26 monthly CH₄ fluxes in the region of influence of the tower for all three years. Using two
27 different distribution maps of CH₄ emissions we determine that average CH₄ emissions over
28 Alaska in summer range between 3 and 8 mg CH₄ m⁻²d⁻¹, albeit with large uncertainties
29 stemming from the large uncertainty in the background. The modeled enhancements do not
30 correlate well with observations, however, indicating that a model with a more accurate
31 spatial and temporal distribution of CH₄ fluxes is needed. The tower observations also
32 indicate that there are no significant differences between the three years. This simple analysis

1 provides a flux estimate range that applies as an average over a very large area of Alaska (Fig.
2 1a). CH₄ fluxes in this region are likely to be highly heterogeneous, but our measurements
3 show that the average flux over the entire region is relatively small. This result suggests that
4 although there may be small areas with large fluxes, there are other areas with little to no
5 emissions, or possibly uptake by tundra (Juncher Jorgensen et al., 2015). For this reason, the
6 observations at the tower give context to other flux estimates, from flux towers or chamber
7 studies, for example, that are representative of much smaller areas and are difficult to scale to
8 the larger domain because of high spatial and temporal variability. We also observe CH₄
9 enhancements persisting into the fall (September-October) in all three years, and the analysis
10 shows some CH₄ enhancements in winter and early spring, depending on the year, which may
11 be partially or entirely anthropogenic, based on an analysis of correlations of CH₄ with CO.
12 These late fall and wintertime enhancements, and their large uncertainties in this analysis,
13 demonstrate the need for year-round in-situ observations in the high northern latitudes.

14 The CARVE tower site provides a continuous observation platform that will contribute to
15 future efforts to investigate the high-latitude carbon cycle and its response to warming. As a
16 long-term measurement site with a large regional coverage it will provide understanding of
17 changing emissions in interior Alaska. Our analysis of the years 2012-2014 indicates no
18 measurable change in emissions influencing this site over this period. These tower
19 observations are sensitive to changes in emissions and provide the capability to detect such
20 changes in the future. However, the location of the CARVE tower prohibits any
21 quantification or observation of processes on the North Slope, indicating that additional long-
22 term observation sites with large regional coverage are required north of the Brooks Range of
23 Alaska to detect changes in emissions in the higher northern latitudes. Future efforts will
24 combine the observations from the CARVE tower with other aircraft and ground-based
25 observations in a formal inversion framework to solve for spatially and temporally resolved
26 CH₄ and CO₂ fluxes in Alaska.

27 **Data availability**

28 All the tower observations and WRF-STILT footprints used in our analysis are publicly
29 available on the CARVE data portal at <https://ilma.jpl.nasa.gov/portal/>. They are also
30 archived at the U.S. Oak Ridge National Laboratory Distributed Active Archive Center for
31 Biogeochemical Dynamics (ORNL DAAC, <https://daac.ornl.gov>).

32

1

2 **Acknowledgements**

3 The research described in this paper was performed for the Carbon in Arctic Reservoirs
4 Vulnerability Experiment (CARVE), an Earth Ventures (EV-1) investigation, under contract
5 with the National Aeronautics and Space Administration. Part of the research described in this
6 paper was performed at the Jet Propulsion Laboratory, California Institute of Technology,
7 under contract with the National Aeronautics and Space Administration. Computing resources
8 for this work were provided by the NASA High-End Computing Program through the NASA
9 Advanced Supercomputing Division at Ames Research Center.

10 The authors would like to acknowledge the invaluable assistance of the NOAA/NESDIS
11 personnel in Fox, Alaska: Marc Meindl and Frank Holan for changing flask packages and
12 high-pressure cylinders throughout the year and providing expert technical assistance when
13 needed, conducting repairs and replacing equipment; Tom Narow and Sean Meyn for
14 providing the Ethernet link and assistance with site networking; Robert Cox, Bonnie Croskey,
15 and Lisa Auvil for shipping out flask packages and cylinders; and Larry Ledlow for allowing
16 the CARVE project to use the site. We thank Jack Higgs, Eric Moglia, Molly Crotwell, Pat
17 Lang, and Duane Kitzis at NOAA/ESRL for providing logistics support, flask packages and
18 shipments, data flagging assistance, and cylinder calibrations for the site. We thank Matt
19 Pender for on-site support, Sean Hardman (JPL) for making the CARVE public data portal,
20 and Kathryn McKain (NOAA/ESRL), Jonathan Kofler (NOAA/ESRL), Rachel Chang
21 (Dalhousie University) and the CARVE Science Team for valuable discussions contributing
22 to the manuscript.

23

1 **References**

- 2 Bruhwiler, L., Dlugokencky, E., Masarie, K., Ishizawa, M., Andrews, A., Miller, J., Sweeney,
3 C., Tans, P., and Worthy, D.: CarbonTracker-CH4: an assimilation system for estimating
4 emissions of atmospheric methane, *Atmos. Chem. Phys.*, 14, 8269-8293, 10.5194/acp-14-
5 8269-2014, 2014.
- 6 CarbonTracker CT2013B: <http://www.esrl.noaa.gov/gmd/ccgg/carbontracker/>, access:
7 October 17, 2013.
- 8 Chang, R. Y. W., Miller, C. E., Dinardo, S. J., Karion, A., Sweeney, C., Daube, B. C.,
9 Henderson, J. M., Mountain, M. E., Eluszkiewicz, J., Miller, J. B., Bruhwiler, L. M. P., and
10 Wofsy, S. C.: Methane emissions from Alaska in 2012 from CARVE airborne observations,
11 *Proc. Natl. Acad. Sci. U. S. A.*, 111, 16694-16699, 10.1073/pnas.1412953111, 2014.
- 12 Chen, H., Karion, A., Rella, C. W., Winderlich, J., Gerbig, C., Filges, A., Newberger, T.,
13 Sweeney, C., and Tans, P. P.: Accurate measurements of carbon monoxide in humid air using
14 the cavity ring-down spectroscopy (CRDS) technique, *Atmos. Meas. Tech.*, 6, 1031-1040,
15 10.5194/amt-6-1031-2013, 2013.
- 16 Dlugokencky, E. J., Myers, R. C., Lang, P. M., Masarie, K. A., Crotwell, A. M., Thoning, K.
17 W., Hall, B. D., Elkins, J. W., and Steele, L. P.: Conversion of NOAA atmospheric dry air
18 CH₄ mole fractions to a gravimetrically prepared standard scale, *Journal of Geophysical*
19 *Research: Atmospheres*, 110, D18306, 10.1029/2005JD006035, 2005.
- 20 Dlugokencky, E. J., Bruhwiler, L., White, J. W. C., Emmons, L. K., Novelli, P. C., Montzka,
21 S. A., Masarie, K. A., Lang, P. M., Crotwell, A. M., Miller, J. B., and Gatti, L. V.:
22 Observational constraints on recent increases in the atmospheric CH₄ burden, *Geophys. Res.*
23 *Let.*, 36, 10.1029/2009gl039780, 2009.
- 24 Euskirchen, E. S., Edgar, C. W., Turetsky, M. R., Waldrop, M. P., and Harden, J. W.:
25 Differential response of carbon fluxes to climate in three peatland ecosystems that vary in the
26 presence and stability of permafrost, *Journal of Geophysical Research: Biogeosciences*, 119,
27 1576-1595, 10.1002/2014JG002683, 2014.
- 28 Fan, S. M., Wofsy, S. C., Bakwin, P. S., Jacob, D. J., Anderson, S. M., Keabian, P. L.,
29 McManus, J. B., Kolb, C. E., and Fitzjarrald, D. R.: Micrometeorological measurements of
30 CH₄ and CO₂ exchange between the atmosphere and subarctic tundra, *Journal of*
31 *Geophysical Research: Atmospheres*, 97, 16627-16643, 10.1029/91JD02531, 1992.
- 32 GLOBE Task Team and others (Hastings, D. A., Paula K. Dunbar, Gerald M. Elphinstone,,
33 Mark Bootz, H. M., Hiroshi Maruyama, Hiroshi Masaharu, Peter Holland, John, Payne, N. A.
34 B., Thomas L. Logan, J.-P. Muller, Gunter Schreier, and John S., and MacDonald): The
35 Global Land One-kilometer Base Elevation (GLOBE) Digital Elevation Model, Version 1.0.,
36 edited by: National Oceanic and Atmospheric Administration, N. G. D. C., 325 Broadway,
37 Boulder, Colorado 80303, 1999.
- 38 Harriss, R. C., Sachse, G. W., Hill, G. F., Wade, L., Bartlett, K. B., Collins, J. E., Steele, L.
39 P., and Novelli, P. C.: Carbon monoxide and methane in the North American Arctic and sub-
40 arctic troposphere - July- August 1988, *J. Geophys. Res.-Atmos.*, 97, 16589-16599, 1992.
- 41 Hayes, D. J., Kicklighter, D. W., McGuire, A. D., Chen, M., Zhuang, Q., Yuan, F., Melillo, J.
42 M., and Wullschlegel, S. D.: The impacts of recent permafrost thaw on land-atmosphere
43 greenhouse gas exchange, *Environmental Research Letters*, 9, 045005, 2014.

- 1 Henderson, J. M., Eluszkiewicz, J., Mountain, M. E., Nehrkorn, T., Chang, R. Y. W., Karion,
2 A., Miller, J. B., Sweeney, C., Steiner, N., Wofsy, S. C., and Miller, C. E.: Atmospheric
3 transport simulations in support of the Carbon in Arctic Reservoirs Vulnerability Experiment
4 (CARVE), *Atmos. Chem. Phys.*, 15, 4093-4116, 10.5194/acp-15-4093-2015, 2015.
- 5 Homer, C. G., Dewitz, J. A., Yang, L., Jin, S., Danielson, P., Xian, G., Coulston, J., Herold,
6 N. D., Wickham, J. D., and Megown, K.: Completion of the 2011 National Land Cover
7 Database for the conterminous United States-Representing a decade of land cover change
8 information., *Photogrammetric Engineering and Remote Sensing*, 81, 345-354, 2015.
- 9 IPCC: Climate Change 2013: The Physical Science Basis. Contribution of Working Group I
10 to the Fourth Assessment Report of the Intergovernmental Panel on Climate Change.,
11 Cambridge University Press, Cambridge, United Kingdom and New York, NY, USA, 1535,
12 2013.
- 13 Iwata, H., Harazono, Y., Ueyama, M., Sakabe, A., Nagano, H., Kosugi, Y., Takahashi, K.,
14 and Kim, Y.: Methane exchange in a poorly-drained black spruce forest over permafrost
15 observed using the eddy covariance technique, *Agricultural and Forest Meteorology*, 214–
16 215, 157-168, <http://dx.doi.org/10.1016/j.agrformet.2015.08.252>, 2015.
- 17 Jeong, S., Hsu, Y.-K., Andrews, A. E., Bianco, L., Vaca, P., Wilczak, J. M., and Fischer, M.
18 L.: A multitower measurement network estimate of California's methane emissions, *Journal of*
19 *Geophysical Research: Atmospheres*, 118, 2013JD019820, 10.1002/jgrd.50854, 2013.
- 20 Johnston, C. E., Ewing, S. A., Harden, J. W., Varner, R. K., Wickland, K. P., Koch, J. C.,
21 Fuller, C. C., Manies, K., and Jorgenson, M. T.: Effect of permafrost thaw on CO₂ and CH₄
22 exchange in a western Alaska peatland chronosequence, *Environmental Research Letters*, 9,
23 085004, 2014.
- 24 Juncher Jorgensen, C., Lund Johansen, K. M., Westergaard-Nielsen, A., and Elberling, B.:
25 Net regional methane sink in High Arctic soils of northeast Greenland, *Nature Geosci*, 8, 20–
26 23, 10.1038/ngeo2305, 2015.
- 27 Kirschke, S., Bousquet, P., Ciais, P., Saunois, M., Canadell, J. G., Dlugokencky, E. J.,
28 Bergamaschi, P., Bergmann, D., Blake, D. R., Bruhwiler, L., Cameron-Smith, P., Castaldi, S.,
29 Chevallier, F., Feng, L., Fraser, A., Heimann, M., Hodson, E. L., Houweling, S., Josse, B.,
30 Fraser, P. J., Krummel, P. B., Lamarque, J.-F., Langenfelds, R. L., Le Quere, C., Naik, V.,
31 O'Doherty, S., Palmer, P. I., Pison, I., Plummer, D., Poulter, B., Prinn, R. G., Rigby, M.,
32 Ringeval, B., Santini, M., Schmidt, M., Shindell, D. T., Simpson, I. J., Spahni, R., Steele, L.
33 P., Strode, S. A., Sudo, K., Szopa, S., van der Werf, G. R., Voulgarakis, A., van Weele, M.,
34 Weiss, R. F., Williams, J. E., and Zeng, G.: Three decades of global methane sources and
35 sinks, *Nature Geosci*, 6, 813-823, 10.1038/ngeo1955, 2013.
- 36 Kort, E. A., Eluszkiewicz, J., Stephens, B. B., Miller, J. B., Gerbig, C., Nehrkorn, T., Daube,
37 B. C., Kaplan, J. O., Houweling, S., and Wofsy, S. C.: Emissions of CH₄ and N₂O over the
38 United States and Canada based on a receptor-oriented modeling framework and COBRA-NA
39 atmospheric observations, *Geophys. Res. Lett.*, 35, 5, 10.1029/2008gl034031, 2008.
- 40 Lin, J. C., Gerbig, C., Wofsy, S. C., Andrews, A. E., Daube, B. C., Davis, K. J., and Grainger,
41 C. A.: A near-field tool for simulating the upstream influence of atmospheric observations:
42 The Stochastic Time-Inverted Lagrangian Transport (STILT) model, *Journal of Geophysical*
43 *Research: Atmospheres*, 108, 4493, 10.1029/2002JD003161, 2003.
- 44 Lin, J. C., Brunner, D., Gerbig, C., Stohl, A., Luhar, A. K., and Webley, P. W.: Lagrangian
45 Modeling of the Atmosphere, Vol. 200, American Geophysical Union, 349 pp., 2012.

- 1 Luus, K. A., and Lin, J. C.: The Polar Vegetation Photosynthesis and Respiration Model: a
2 parsimonious, satellite-data-driven model of high-latitude CO₂ exchange, *Geosci. Model*
3 *Dev.*, 8, 2655-2674, 10.5194/gmd-8-2655-2015, 2015.
- 4 Mastepanov, M., Sigsgaard, C., Dlugokencky, E. J., Houweling, S., Strom, L., Tamstorf, M.
5 P., and Christensen, T. R.: Large tundra methane burst during onset of freezing, *Nature*, 456,
6 628-U658, 10.1038/nature07464, 2008.
- 7 McGuire, A. D., Anderson, L. G., Christensen, T. R., Dallimore, S., Guo, L. D., Hayes, D. J.,
8 Heimann, M., Lorenson, T. D., Macdonald, R. W., and Roulet, N.: Sensitivity of the carbon
9 cycle in the Arctic to climate change, *Ecol. Monogr.*, 79, 523-555, 2009.
- 10 McGuire, A. D., Hayes, D. J., Kicklighter, D. W., Manizza, M., Zhuang, Q., Chen, M.,
11 Follows, M. J., Gurney, K. R., McClelland, J. W., Melillo, J. M., Peterson, B. J., and Prinn, R.
12 G.: An analysis of the carbon balance of the Arctic Basin from 1997 to 2006, *Tellus Ser. B-*
13 *Chem. Phys. Meteorol.*, 62, 455-474, 10.1111/j.1600-0889.2010.00497.x, 2010.
- 14 McKain, K., Down, A., Raciti, S. M., Budney, J., Hutyra, L. R., Floerchinger, C., Herndon, S.
15 C., Nehrkorn, T., Zahniser, M. S., Jackson, R. B., Phillips, N., and Wofsy, S. C.: Methane
16 emissions from natural gas infrastructure and use in the urban region of Boston,
17 Massachusetts, *Proceedings of the National Academy of Sciences*, 112, 1941-1946,
18 10.1073/pnas.1416261112, 2015.
- 19 Mesinger, F., DiMego, G., Kalnay, E., Mitchell, K., Shafran, P. C., Ebisuzaki, W., Jović, D.,
20 Woollen, J., Rogers, E., Berbery, E. H., Ek, M. B., Fan, Y., Grumbine, R., Higgins, W., Li,
21 H., Lin, Y., Manikin, G., Parrish, D., and Shi, W.: North American Regional Reanalysis,
22 *Bulletin of the American Meteorological Society*, 87, 343-360, 10.1175/BAMS-87-3-343,
23 2006.
- 24 Miller, S. M., Worthy, D. E. J., Michalak, A. M., Wofsy, S. C., Kort, E. A., Havice, T. C.,
25 Andrews, A. E., Dlugokencky, E. J., Kaplan, J. O., Levi, P. J., Tian, H., and Zhang, B.:
26 Observational constraints on the distribution, seasonality, and environmental predictors of
27 North American boreal methane emissions, *Glob. Biogeochem. Cycle*, 28, 146-160,
28 10.1002/2013GB004580, 2014.
- 29 Morrissey, L. A., and Livingston, G. P.: Methane emissions from Alaska Arctic tundra: An
30 assessment of local spatial variability, *Journal of Geophysical Research: Atmospheres*, 97,
31 16661-16670, 10.1029/92JD00063, 1992.
- 32 Nehrkorn, T., Eluszkiewicz, J., Wofsy, S., Lin, J., Gerbig, C., Longo, M., and Freitas, S.:
33 Coupled weather research and forecasting–stochastic time-inverted lagrangian transport
34 (WRF–STILT) model, *Meteorol Atmos Phys*, 107, 51-64, 10.1007/s00703-010-0068-x, 2010.
- 35 O'Connor, F. M., Boucher, O., Gedney, N., Jones, C. D., Folberth, G. A., Coppell, R.,
36 Friedlingstein, P., Collins, W. J., Chappellaz, J., Ridley, J., and Johnson, C. E.: Possible role
37 of wetlands, permafrost, and methane hydrates in the methane cycle under future climate
38 change: A review, *Rev. Geophys.*, 48, RG4005, 10.1029/2010rg000326, 2010.
- 39 Oechel, W. C., Hastings, S. J., Vourlitis, G., Jenkins, M., Riechers, G., and Grulke, N.: Recent
40 change of Arctic tundra ecosystems from a net carbon dioxide sink to a source, *Nature*, 361,
41 520-523, 1993.
- 42 Olefeldt, D., Turetsky, M. R., Crill, P. M., and McGuire, A. D.: Environmental and physical
43 controls on northern terrestrial methane emissions across permafrost zones, *Glob. Change*
44 *Biol.*, 19, 589-603, 10.1111/gcb.12071, 2013.

1 Rella, C. W., Chen, H., Andrews, A. E., Filges, A., Gerbig, C., Hatakka, J., Karion, A., Miles,
2 N. L., Richardson, S. J., Steinbacher, M., Sweeney, C., Wastine, B., and Zellweger, C.: High
3 accuracy measurements of dry mole fractions of carbon dioxide and methane in humid air,
4 *Atmos. Meas. Tech.*, 6, 837-860, 10.5194/amt-6-837-2013, 2013.

5 Riggs, G., and Hall, D.: MODIS snow and ice products, and their assessment and
6 applications, in: *Land Remote Sensing and Global Environmental Change, Remote Sensing
7 and Digital Image Processing*, edited by: Ramachandran, B., Justice, C. O., and Abrams, M.
8 J., 11, 681-707, 2011.

9 Sasakawa, M., Shimoyama, K., Machida, T., Tsuda, N., Suto, H., Arshinov, M., Davydov, D.,
10 Fofonov, A., Krasnov, O., Saeki, T., Koyama, Y., and Maksyutov, S.: Continuous
11 measurements of methane from a tower network over Siberia, *Tellus B*, 62, 403-416,
12 10.1111/j.1600-0889.2010.00494.x, 2010.

13 Sasakawa, M., Machida, T., Tsuda, N., Arshinov, M., Davydov, D., Fofonov, A., and
14 Krasnov, O.: Aircraft and tower measurements of CO₂ concentration in the planetary
15 boundary layer and the lower free troposphere over southern taiga in West Siberia: Long-term
16 records from 2002 to 2011, *J. Geophys. Res.-Atmos.*, 118, 9489-9498, 10.1002/jgrd.50755,
17 2013.

18 Schuur, E. A. G., Bockheim, J., Canadell, J. G., Euskirchen, E., Field, C. B., Goryachkin, S.
19 V., Hagemann, S., Kuhry, P., Lafleur, P. M., Lee, H., Mazhitova, G., Nelson, F. E., Rinke, A.,
20 Romanovsky, V. E., Shiklomanov, N., Tarnocai, C., Venevsky, S., Vogel, J. G., and Zimov,
21 S. A.: Vulnerability of permafrost carbon to climate change: Implications for the global
22 carbon cycle, *Bioscience*, 58, 701-714, 10.1641/b580807, 2008.

23 Schuur, E. A. G., Vogel, J. G., Crummer, K. G., Lee, H., Sickman, J. O., and Osterkamp, T.
24 E.: The effect of permafrost thaw on old carbon release and net carbon exchange from tundra,
25 *Nature*, 459, 556-559, 10.1038/nature08031, 2009.

26 Schuur, E. A. G., McGuire, A. D., Schadel, C., Grosse, G., Harden, J. W., Hayes, D. J.,
27 Hugelius, G., Koven, C. D., Kuhry, P., Lawrence, D. M., Natali, S. M., Olefeldt, D.,
28 Romanovsky, V. E., Schaefer, K., Turetsky, M. R., Treat, C. C., and Vonk, J. E.: Climate
29 change and the permafrost carbon feedback, *Nature*, 520, 171-179, 10.1038/nature14338,
30 2015.

31 Skamarock, W. C., Klemp, J. B., Dudhia, J., Gill, D. O., Barker, D. M., Duda, M. G., Wang,
32 X.-Y., Wang, W., and Powers, J. G.: A Description of the Advanced Research WRF Version
33 3, Technical Note 475+STR, MMM Division, NCAR, Boulder, CO, USA, 133, 2008.

34 MODIS Vegetation Indices (MOD13) C5 Users's Guide, Terrestrial Biophysics and Remote
35 Sensing Lab, The University of Arizona: <http://www.ctahr.hawaii.edu/grem/modis-ug.pdf>,
36 access: September 7, 2010.

37 Sweeney, C., Karion, A., Wolter, S., Newberger, T., Guenther, D., Higgs, J. A., Andrews, A.
38 E., Lang, P. M., Neff, D., Dlugokencky, E., Miller, J. B., Montzka, S. A., Miller, B. R.,
39 Masarie, K. A., Biraud, S. C., Novelli, P. C., Crotwell, M., Crotwell, A. M., Thoning, K., and
40 Tans, P. P.: Seasonal climatology of CO₂ across North America from aircraft measurements
41 in the NOAA/ESRL Global Greenhouse Gas Reference Network, *Journal of Geophysical
42 Research: Atmospheres*, n/a-n/a, 10.1002/2014JD022591, 2015.

43 von Fischer, J. C., Rhew, R. C., Ames, G. M., Fossick, B. K., and von Fischer, P. E.:
44 Vegetation height and other controls of spatial variability in methane emissions from the

1 Arctic coastal tundra at Barrow, Alaska, *Journal of Geophysical Research: Biogeosciences*,
2 115, n/a-n/a, 10.1029/2009JG001283, 2010.

3 Walter, K. M., Smith, L. C., and Chapin, F. S.: Methane bubbling from northern lakes:
4 present and future contributions to the global methane budget, *Philosophical Transactions of*
5 *the Royal Society a-Mathematical Physical and Engineering Sciences*, 365, 1657-1676,
6 10.1098/rsta.2007.2036, 2007.

7 Whalen, S. C., and Reeburgh, W. S.: A methane flux time series for tundra environments,
8 *Glob. Biogeochem. Cycle*, 2, 399-409, 10.1029/GB002i004p00399, 1988.

9 Wilson, A. B., Bromwich, D. H., and Hines, K. M.: Evaluation of Polar WRF forecasts on the
10 Arctic System Reanalysis domain: Surface and upper air analysis, *Journal of Geophysical*
11 *Research: Atmospheres*, 116, 10.1029/2010JD015013, 2011.

12 Winderlich, J., Chen, H., Gerbig, C., Seifert, T., Kolle, O., Lavric, J. V., Kaiser, C., Hofer, A.,
13 and Heimann, M.: Continuous low-maintenance CO₂/CH₄/H₂O measurements at the Zotino
14 Tall Tower Observatory (ZOTTO) in Central Siberia, *Atmos. Meas. Tech.*, 3, 1113-1128,
15 10.5194/amt-3-1113-2010, 2010.

16 Winderlich, J., Gerbig, C., Kolle, O., and Heimann, M.: Inferences from CO₂ and CH₄
17 concentration profiles at the Zotino Tall Tower Observatory (ZOTTO) on regional
18 summertime ecosystem fluxes, *Biogeosciences*, 11, 2055-2068, 10.5194/bg-11-2055-2014,
19 2014.

20 Worthy, D., Taylor, C., Dlugokencky, E. J., Chan, E., Nisbet, E. G., and Laurila, T.: AMAP
21 Assessment 2015: Methane as an Arctic climate forcer, Chapter 6: Long-term monitoring of
22 atmospheric methane., Arctic Monitoring and Assessment Programme (AMAP), Oslo,
23 Norway. <http://www.amap.no/documents/download/2499>, 61-75, 2015.

24 Zhao, C. L., and Tans, P. P.: Estimating uncertainty of the WMO mole fraction scale for
25 carbon dioxide in air, *Journal of Geophysical Research*, 111, D08S09,
26 10.1029/2005jd006003, 2006.

27 Zona, D., Gioli, B., Commane, R., Lindaas, J., Wofsy, S. C., Miller, C. E., Dinardo, S. J.,
28 Dengel, S., Sweeney, C., Karion, A., Chang, R. Y.-W., Henderson, J. M., Murphy, P. C.,
29 Goodrich, J. P., Moreaux, V., Liljedahl, A., Watts, J. D., Kimball, J. S., Lipson, D. A., and
30 Oechel, W. C.: Cold season emissions dominate the Arctic tundra methane budget,
31 *Proceedings of the National Academy of Sciences*, 113, 40-45, 10.1073/pnas.1516017113,
32 2016.

33

34

35

1

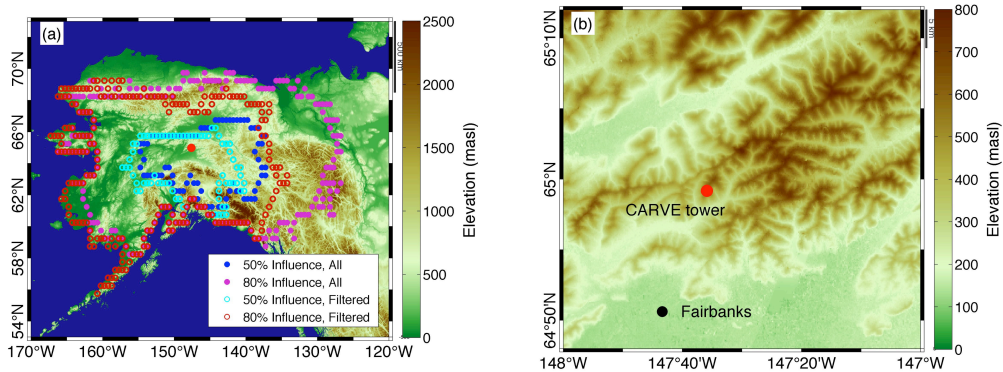
2 Table 1. Coefficient of determination (R^2) between ΔCH_4 and ΔCO in each month. Months
3 with $R^2 > 0.2$ are in bold.

	Jan	Feb	Mar	Apr	May	Jun	Jul	Aug	Sep	Oct	Nov	Dec
2012	0.30	0.14	0.12	0.16	0.81	0.00	0.00	0.05	0.17	0.22	0.49	NA
2013	0.66	0.14	0.19	0.14	0.26	0.01	0.07	0.01	0.19	0.09	0.01	0.15
2014	0.49	0.67	0.66	0.03	0.17	0.00	0.07	0.00	0.10	0.06	0.10	0.00

4

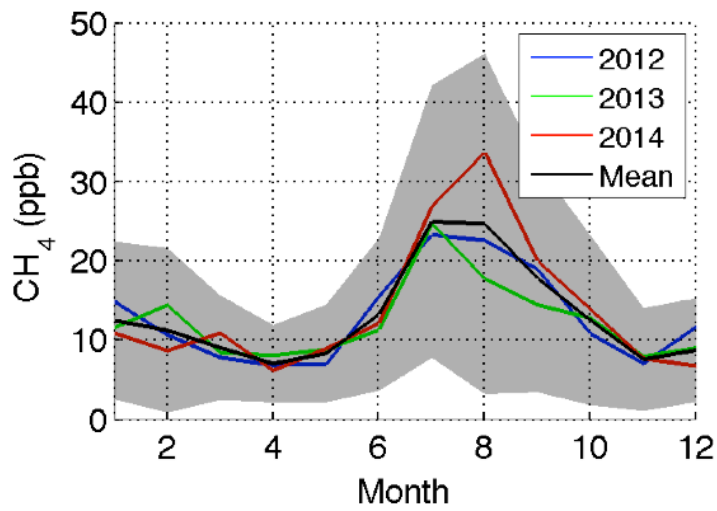
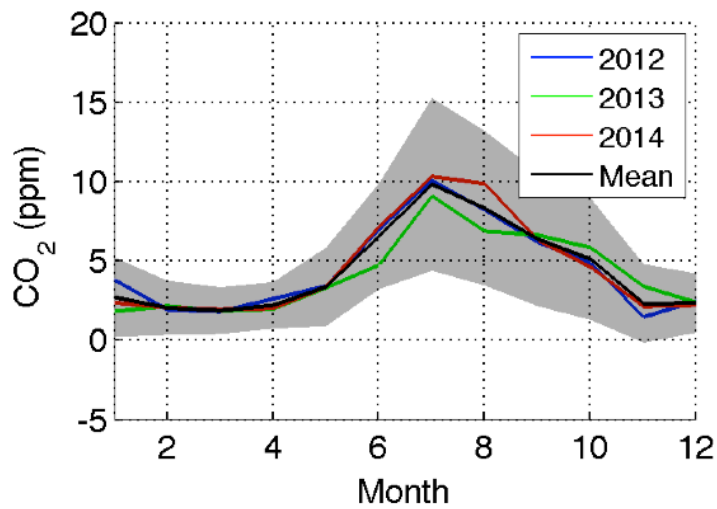
5

1
2



3

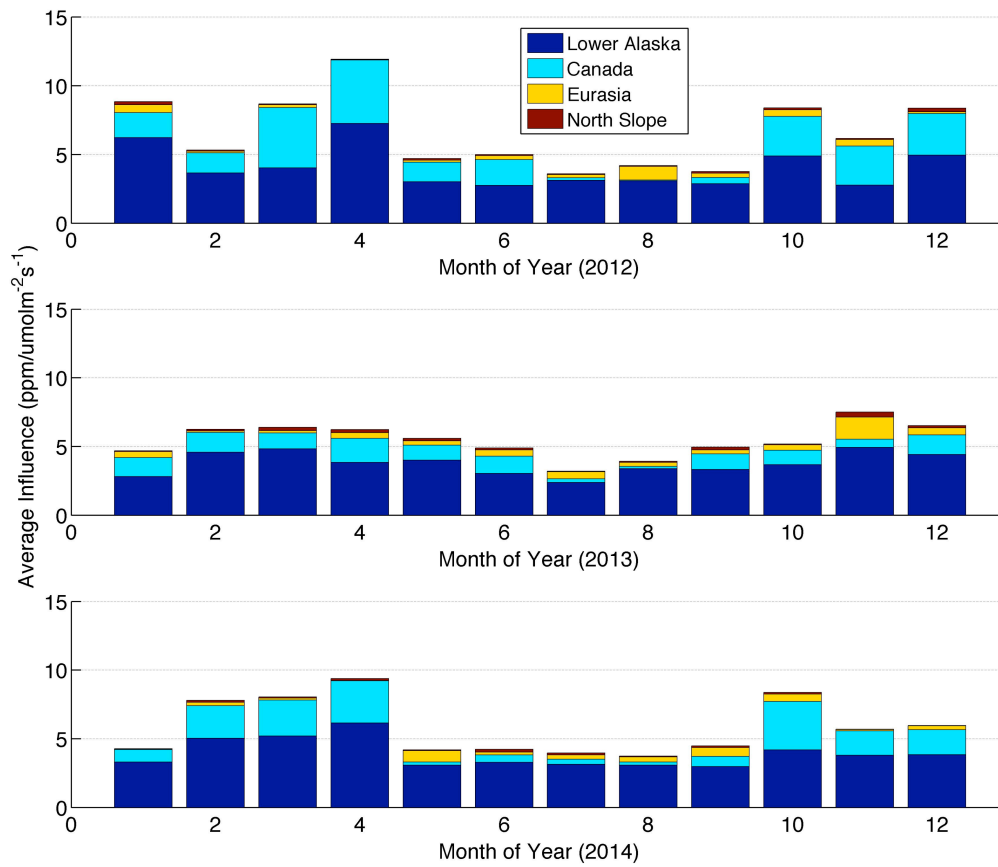
4 Figure 1. CO₂ and CH₄ measurements from the CARVE tower (filled red circle, both panels)
5 have high sensitivity to the boreal forests and lowlands of interior Alaska as shown by the
6 50% (blue) and 80% (purple) surface influence contours for the average WRF-STILT
7 influence functions calculated for mid-afternoon averages over the period 2012-2014 (a). The
8 same influence contours (cyan and red open circles) are shown for the subset of footprints
9 used in the flux analysis after filtering. Note the elevation scale differs between the panels.
10 Elevation data in (a) is from NOAA's National Geophysical Data Center Global Land One-
11 kilometer Base Elevation (GLOBE) Database
12 (<http://www.ngdc.noaa.gov/mgg/topo/report/globedocumentationmanual.pdf>, (GLOBE Task
13 Team and others (Hastings et al., 1999)). High-resolution elevation data in (b) is from
14 ASTER GDEM, a product of METI and NASA.
15



1
2
3
4
5
6
7
8

Figure 2. Mean monthly diurnal cycle amplitude of hourly averaged CO₂ (top) and CH₄ (bottom). The average over three full calendar years (2012-2014) is shown in black with the gray shading indicating one standard deviation of each month's average. The average diurnal cycles for each individual year are indicated by the blue (2012), green (2013) and red (2014) solid lines.

1

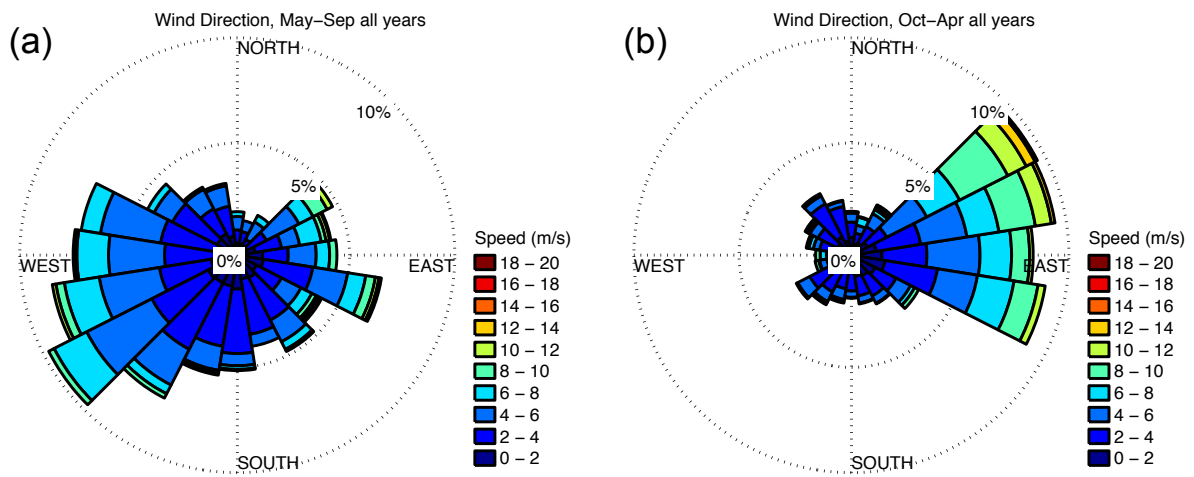


2

3 Figure 3. Magnitude of land surface influence on the tower measurements, in ppm/($\mu\text{mol m}^{-2}$
4 s^{-1}), for average monthly mid-afternoon footprints from the WRF-STILT model, for 2012
5 (top), 2013 (middle), and 2014 (bottom). Colors, as indicated in the figure legend, show the
6 average monthly surface influence of Lower Alaska (defined as any part of Alaska south of
7 the Brooks Range, i.e. not part of the North Slope), Canada, Eurasia, and the North Slope of
8 Alaska.

9

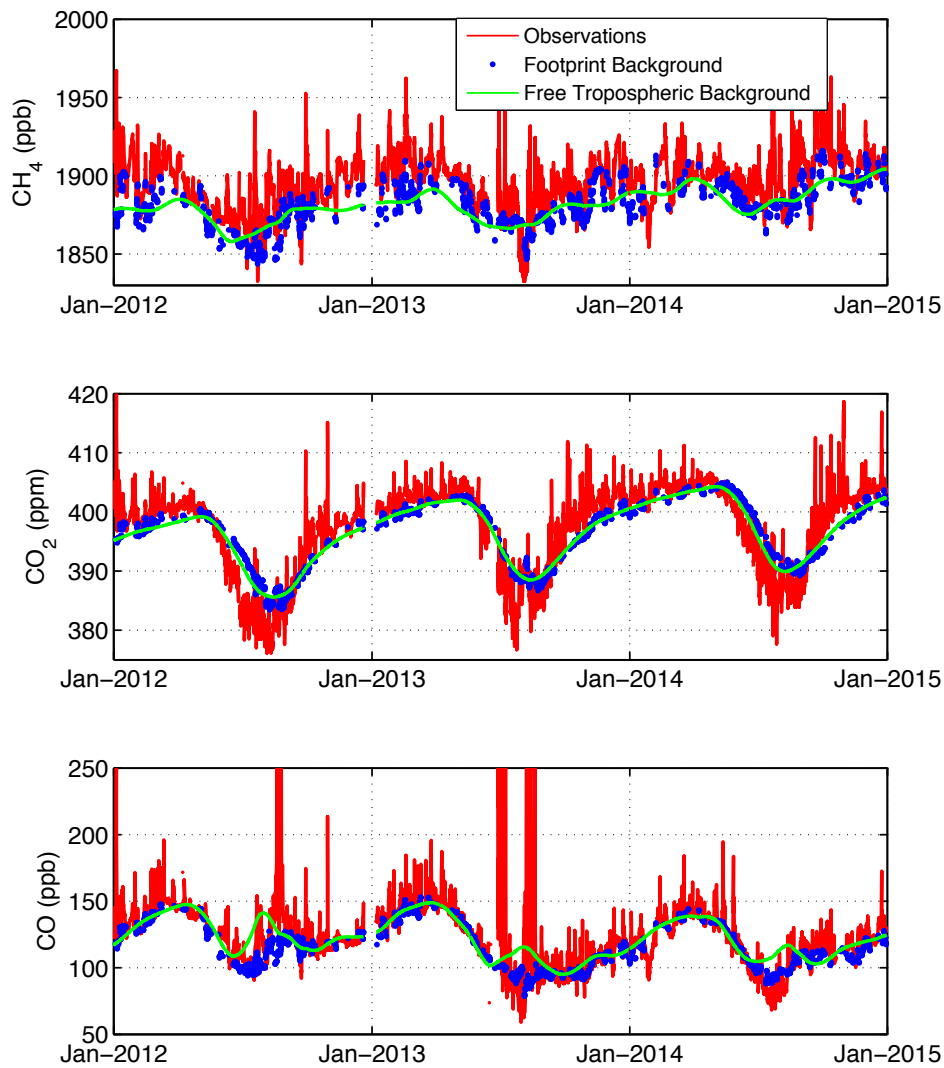
1
2



3
4
5
6
7

Figure 4. Wind roses for the tower averaged over (a) May-September and (b) October-April for all three years during mid-afternoon hours, from the 2D sonic anemometer at the 32 magl level of the tower.

1

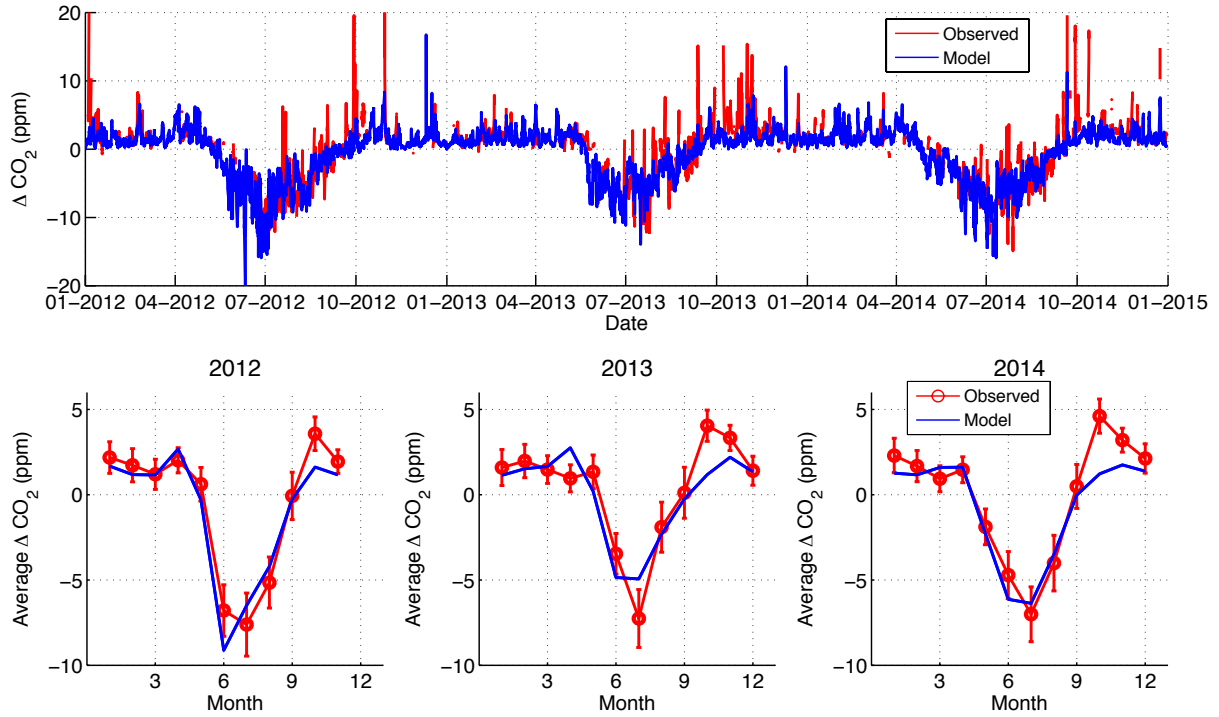


2

3 Figure 5. Time series of hourly average observed mole fractions (red) and background mole
4 fractions (blue), 1 pm to 6 pm local standard time (LST) only for CH₄ (top), CO₂ (center), and
5 CO (lower) at the CARVE tower. Observations are indicated by solid red lines, while the
6 background mole fractions used for this analysis are shown in blue dots, and are derived using
7 the particle trajectories from the STILT model and an empirical Pacific boundary curtain,
8 described in the text. Gaps in the blue dots appear when the background could not be
9 calculated using the model because the air masses did not enter the domain from the West (as
10 described in Sect. 3.3). The green line represents the value of the same Pacific boundary
11 curtain at the site latitude (65°N) at 3500 meters above sea level, i.e. the free troposphere. The
12 vertical scale for CO has been truncated.

13

1

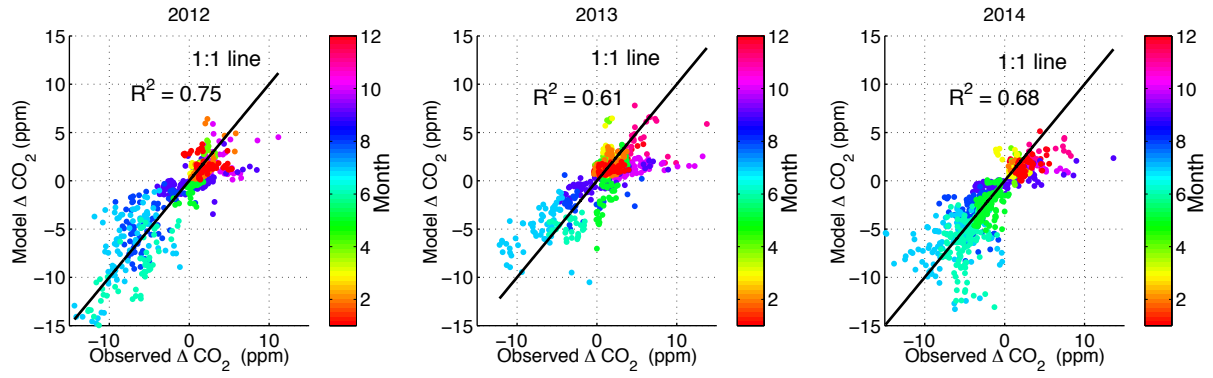


2

3 Figure 6. Top: ΔCO_2 observed (i.e. observations minus background, red), along with the
4 modeled ΔCO_2 convolution (blue). Bottom: Monthly average comparisons between the model
5 (blue) and observations (red line and circles) for each year. Error bars on the observations
6 represent the average background uncertainty.

7

1

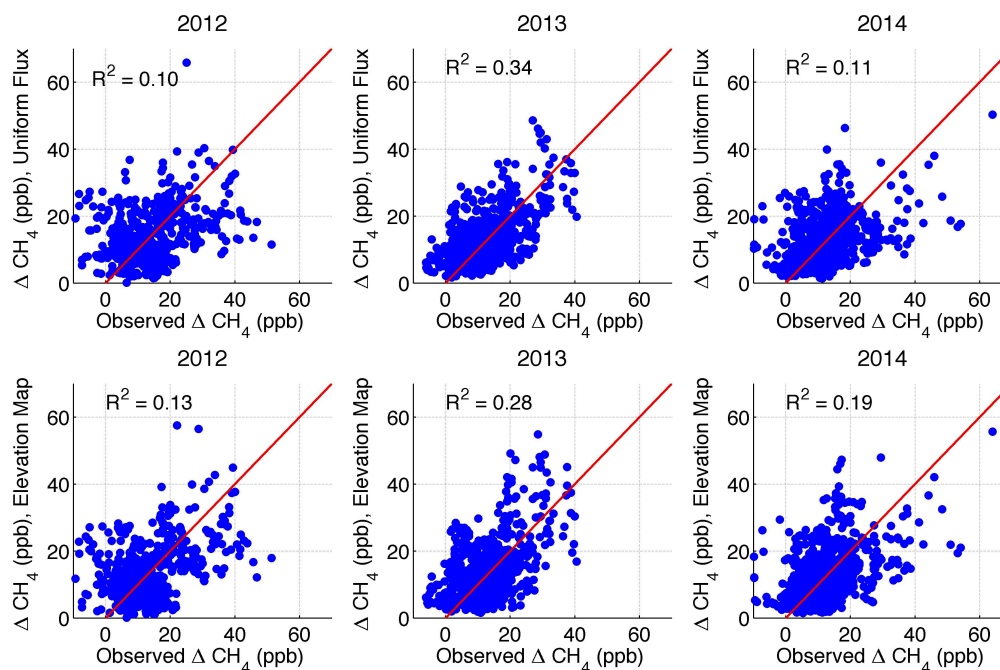


2

3 Figure 7. Correlation between observed and modeled ΔCO_2 , for 2012 (left), 2013 (center),
4 and 2014 (right), colored by month. The coefficient of determination, R^2 , is indicated in each
5 plot, along with the one-to-one line. Data points represent hourly averages between 1 pm and
6 6 pm LST and filtered according to criteria described in the text.

7

1

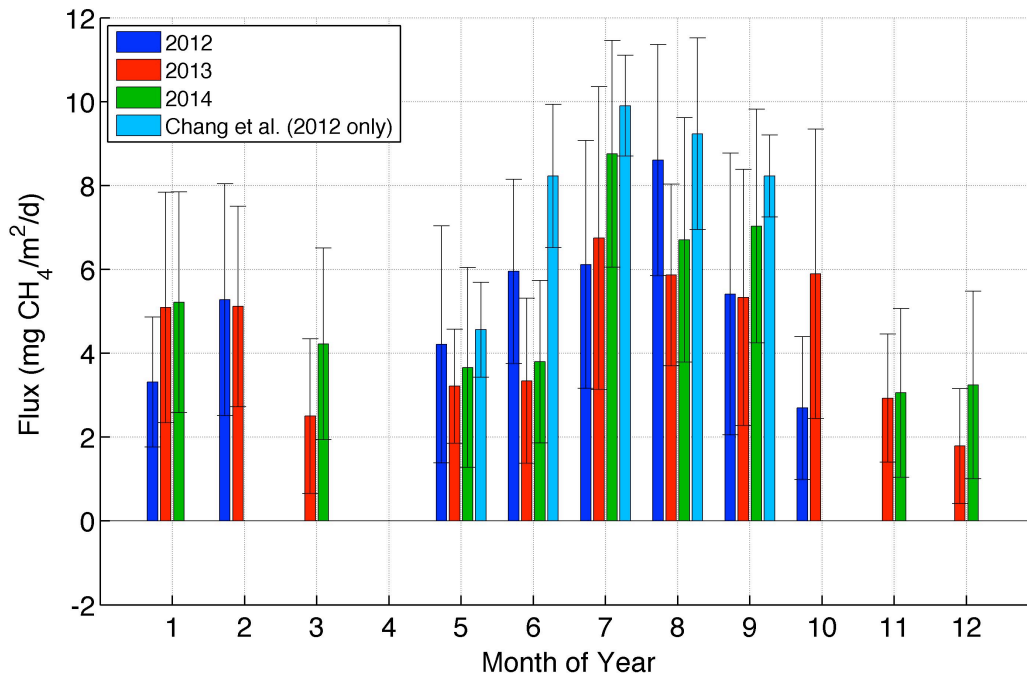


2

3 Figure 8. Optimized model ΔCH_4 (ppb) for the scaled uniform flux (top row) and scaled
4 elevation-based flux map (bottom row), for 2012 (left), 2013 (center), 2014 (right), all plotted
5 against observed ΔCH_4 . Fluxes were scaled to match monthly average observed ΔCH_4 with
6 monthly scaling factors. The coefficient of determination, R^2 , is indicated in each plot, along
7 with the one-to-one line. Data points represent hourly averages between 1 pm and 6 pm LST
8 and filtered according to criteria described in the text.

9

1
2



3

4 Figure 9. Average Alaska monthly CH₄ fluxes for 2012 (blue), 2013 (red), and 2014 (green),
5 estimated based on a uniform Alaska-wide flux scaled to monthly mean observations at the
6 CRV tower. Light blue bars indicate monthly fluxes derived from 2012 CARVE aircraft
7 observations, with error bars representing the 68% confidence interval (CI), (calculated by
8 dividing the 95% CI by 1.96), from Chang et al. (2014). Error bars on the tower-derived
9 fluxes are based on propagating background uncertainty (1-sigma, Sect. 3.3) and uncertainty
10 derived from a sensitivity analysis on the altitude of the model runs (Sect. 3.2) only. Months
11 for which fluxes were based on six or fewer days were eliminated from the analysis.